



HAL
open science

Optimized effective potential forces with the plane-wave and pseudopotential method

Damian Contant, Maria Hellgren

► **To cite this version:**

Damian Contant, Maria Hellgren. Optimized effective potential forces with the plane-wave and pseudopotential method. *Physical Review B*, 2024, 110 (12), pp.125110. 10.1103/PhysRevB.110.125110 . hal-04781977

HAL Id: hal-04781977

<https://hal.science/hal-04781977v1>

Submitted on 14 Nov 2024

HAL is a multi-disciplinary open access archive for the deposit and dissemination of scientific research documents, whether they are published or not. The documents may come from teaching and research institutions in France or abroad, or from public or private research centers.

L'archive ouverte pluridisciplinaire **HAL**, est destinée au dépôt et à la diffusion de documents scientifiques de niveau recherche, publiés ou non, émanant des établissements d'enseignement et de recherche français ou étrangers, des laboratoires publics ou privés.

Optimized effective potential forces with the plane-wave and pseudopotential method

Damian Contant and Maria Hellgren

Sorbonne Université, MNHN, UMR CNRS 7590, IMPMC, 4 place Jussieu, 75005 Paris, France

(Dated: September 13, 2024)

The optimized effective potential (OEP) approach has so far mainly been used in benchmark studies and for the evaluation of band gaps. In this work, we extend the application of the OEP by determining the analytical ionic forces within the plane-wave and pseudopotential framework. It is first shown that, due to the constrained optimization inherent to the OEP approach, an extra term needs to be added to the standard Hellmann-Feynman expression for the forces, whenever nonlocal pseudopotentials are employed. Computing this term for functionals based on Hartree-Fock and the hybrid PBE0 functional yields forces with excellent numerical accuracy. Furthermore, results for equilibrium geometries and vibrational frequencies on a set of molecules and solids confirm that the local exchange OEP is able to reproduce results obtained with the nonlocal exchange potential. Our work opens up the possibility to study lattice dynamics using advanced orbital functionals for describing exchange and correlation effects.

I. INTRODUCTION

In the field of computational physics, a wide variety of approaches for total energy and force calculations are available. Depending on the application, the accuracy-cost ratio can be an important factor to consider. In this regard, Kohn-Sham (KS) Density Functional Theory (DFT), with a well-chosen functional, is often the preferred approach [1–4].

Within KS-DFT, approximate functionals are sorted into different classes according to their level of description of the exchange-correlation (xc) energy [5–7]. Starting from the local density approximation (LDA), improved functionals include a semilocal dependency through the gradient of the density, and are known as the generalised gradient approximations (GGAs). Adding a dependence on the KS kinetic energy density leads to the non-local meta-GGAs. Each of the above functional classes suffers, more or less, from self-interaction errors due to their approximate description of Hartree-Fock (HF) exchange [8], a problem which can be mitigated with hybrid functionals that mix in a fraction of HF exchange into a semilocal functional [9, 10]. In this way, the KS density matrix is introduced as an additional ingredient in the xc functional. An accurate description of correlation can be found with functionals based on the KS Green’s function that depend on the full KS spectrum. Examples are functionals derived from many-body perturbation theory (MBPT) such as the random phase approximation (RPA) [11].

Meta-GGAs, hybrid and MBPT-based functionals all have an explicit dependency on the KS orbitals, rather than the density. As a consequence, the xc potential, i.e., the functional derivative of the xc energy with respect to the density, does not have an analytical expression. Self-consistent calculations are, therefore, often performed within the generalised KS framework [12–14], or by allowing for larger variational freedom. In the case of hybrid functionals this implies the use of an integral operator, the nonlocal exchange potential [15], and, in the case of meta-GGAs, the use of a differential opera-

tor [16, 17]. The RPA functional has a natural extension within MBPT. Free variations with respect to the many-body Green’s function leads to a nonlocal and energy-dependent potential - the *GW* self-energy [18–20]. Due to the high complexity of such calculations there are only a few reported in the literature [21–24].

In order to remain within the KS formulation, the variational freedom has to be restricted such that the orbitals are generated by a local multiplicative potential. Functional differentiation with respect to the density via the KS orbitals leads to an integral equation, known as the optimized effective potential (OEP) equation, for determining the xc potential numerically [25, 26]. Tests on various systems have demonstrated that the OEP often gives total energies and densities in close agreement with results obtained within the generalised KS scheme [27–29]. On the other hand, except for the highest occupied molecular orbital (HOMO) eigenvalue [30], the spectrum will always be different. The KS virtual orbitals can, for example, be shown to provide a better description of the optical excitation energies [31], but the fundamental gap is strongly underestimated, even with the exact KS potential [32, 33]. One can show that the KS potential must jump with a constant when crossing integer particle numbers in the ensemble formulation of DFT [34]. Adding this constant, or the so-called derivative discontinuity correction, to the KS gap results in the true fundamental gap. Within hybrid functionals, the corrected KS gap is in good agreement with the gap obtained from the generalised KS scheme [35], and same is expected to be true for meta-GGAs [14]. Within RPA, it becomes equivalent to the gap within G_0W_0 theory [36–38].

The numerical solution to the OEP equation has been the subject of numerous studies. A direct solution based on the inversion of the KS density response function is known to present numerical instabilities in Gaussian basis sets [39–41]. These issues are almost absent from OEP calculations resorting to plane-waves [42], real space grids [43, 44], or spline basis sets [20, 45–48]. Furthermore, direct minimization [49] and iterative approaches [50–52] that circumvent the inversion of the KS density response

function have been developed, making routine OEP calculations feasible on a wide range of systems. All-electron studies have focused on the role of the core-valence interaction and concluded that the pseudopotential approximation is valid also for OEP calculations [44, 53–56]. A review on orbital-dependent functionals and their numerical aspects can be found in Ref. 57.

Current applications of the OEP are mostly found in band structure calculations. Either for a direct comparison with experiment [58, 59], or as a starting point for G_0W_0 calculations [35, 38, 60, 61]. In principle, self-consistent OEP calculations also give access to the ionic forces, which are relevant for structural relaxation and phonon spectra. The prospect of using an advanced description of exchange and correlation for calculating these important properties has so far not been much explored. As of now, there are only a few works studying OEP forces on small molecules using Gaussian basis sets [62–64].

In the present study, we investigate the analytical OEP forces using the plane-wave basis set and norm-conserving pseudopotentials, and show that it is possible to achieve excellent numerical accuracy when applied to both molecules and solids.

The paper is organized as follows. In section II, we provide the mathematical details of the OEP approach. In section III, we discuss the OEP forces and their implementation using norm-conserving pseudopotentials. We also analyze the numerical accuracy achieved on various molecules and solids. Finally, in section IV, we exploit the calculated forces to determine equilibrium geometries, the vibrational modes of H_2O and α -quartz, and the phonon dispersion of diamond. The conclusions are given in section V.

II. OPTIMIZED EFFECTIVE POTENTIAL

Similarly to xc functionals depending explicitly on the density and its gradient, orbital-dependent functionals based on the OEP are designed to predict the density and the ground-state energy through a local effective KS potential. The self-consistent procedure does, however, present differences as the OEP KS potential does not have an analytical expression explicit in the orbitals. Instead, the numerical solution of the OEP integral equation is required as an intermediate step in each iteration towards self-consistency.

The ground-state total energy within KS-DFT is written as

$$E_{\text{tot}} = T_s + E_{\text{Hxc}} + \int v_{\text{ext}}(\mathbf{r})n(\mathbf{r}) d\mathbf{r}, \quad (1)$$

where T_s is the kinetic energy of non-interacting electrons moving in an effective KS potential $v_{\text{eff}}(\mathbf{r})$ such that

$$\left\{ -\frac{1}{2}\nabla^2 + v_{\text{eff}}(\mathbf{r}) \right\} \varphi_i(\mathbf{r}) = \epsilon_i \varphi_i(\mathbf{r}). \quad (2)$$

E_{Hxc} is the Hartree (H) and xc energy, and $v_{\text{ext}}(\mathbf{r})$ is the external nuclear potential interacting with the electronic density $n(\mathbf{r})$. Each independent electron is described by a Kohn-Sham orbital φ_i and has the energy ϵ_i . The total energy is minimized when the effective potential is given by

$$v_{\text{eff}}(\mathbf{r}) = v_{\text{ext}}(\mathbf{r}) + v_{\text{Hxc}}(\mathbf{r}) \quad (3)$$

where

$$v_{\text{Hxc}}(\mathbf{r}) = \frac{\delta E_{\text{Hxc}}}{\delta n(\mathbf{r})}. \quad (4)$$

All terms in Eq. (1) can be expressed explicitly in terms of the density except for the KS kinetic energy and the xc part of the Hxc energy. Since the functional dependence of the exact xc energy on the density is unknown, approximations are needed for its evaluation. The OEP method is relevant for xc functionals with an implicit dependence on the density via KS orbitals. In this case, the functional derivative in Eq. (4) is evaluated using the chain rule since the variation of the orbitals with respect to v_{eff} is easy to construct from linear response theory

$$\frac{\delta E_{\text{xc}}}{\delta v_{\text{eff}}(\mathbf{r})} = \int \frac{\delta n(\mathbf{r}')}{\delta v_{\text{eff}}(\mathbf{r})} v_{\text{xc}}(\mathbf{r}', \mathbf{r}) d\mathbf{r}'. \quad (5)$$

Let us now focus on the exact-exchange (EXX) approximation. Within EXX, there is no correlation and the exchange energy functional is identical to the HF exchange energy [28]

$$E_x = -\frac{1}{4} \int \gamma(\mathbf{r}, \mathbf{r}') v(\mathbf{r} - \mathbf{r}') \gamma(\mathbf{r}', \mathbf{r}) d\mathbf{r} d\mathbf{r}'. \quad (6)$$

Assuming closed-shell systems, γ is the first order spin-averaged reduced density matrix and v is the Coulomb interaction. Free variations of the EXX total energy with respect to γ yields the HF equation with the nonlocal HF exchange potential $V_x(\mathbf{r}, \mathbf{r}') = -\frac{1}{2} v(\mathbf{r} - \mathbf{r}') \gamma(\mathbf{r}', \mathbf{r})$ [3]. A variation with respect to a local effective potential corresponds to a minimization of the EXX total energy on a restricted domain of allowed orbitals, and the minimum is found when the exchange part of the effective potential obeys Eq. (5) [25, 26]. We thus need to evaluate the functional derivative of E_x (Eq. (6)) with respect to v_{eff}

$$\frac{\delta E_x}{\delta v_{\text{eff}}(\mathbf{r})} = \int \frac{\delta \gamma(\mathbf{r}', \mathbf{r}'')}{\delta v_{\text{eff}}(\mathbf{r})} V_x(\mathbf{r}', \mathbf{r}'') d\mathbf{r}' d\mathbf{r}''. \quad (7)$$

Combining Eq. (5) and Eq. (7) yields the following integral equation for $v_x(\mathbf{r})$

$$\int \chi_s(\mathbf{r}, \mathbf{r}') v_x(\mathbf{r}') d\mathbf{r}' = \int \Lambda_s(\mathbf{r}, \mathbf{r}', \mathbf{r}'') V_x(\mathbf{r}', \mathbf{r}'') d\mathbf{r}' d\mathbf{r}'', \quad (8)$$

known as the OEP equation. The variation of the electronic density with respect to v_{eff} is equal to the KS linear

density response function and can be written explicitly as

$$\begin{aligned} \chi_s(\mathbf{r}, \mathbf{r}') = & 2 \sum_i^{\text{occ}} \sum_j^{\text{unocc}} \frac{\varphi_j^*(\mathbf{r}') \varphi_j(\mathbf{r}) \varphi_i^*(\mathbf{r}) \varphi_i(\mathbf{r}')}{\epsilon_i - \epsilon_j} \\ & + 2 \sum_i^{\text{occ}} \sum_j^{\text{unocc}} \frac{\varphi_i^*(\mathbf{r}') \varphi_i(\mathbf{r}) \varphi_j^*(\mathbf{r}) \varphi_j(\mathbf{r}')}{\epsilon_i - \epsilon_j}. \end{aligned} \quad (9)$$

The variation of γ with respect to v_{eff} is given by

$$\begin{aligned} \Lambda_s(\mathbf{r}, \mathbf{r}', \mathbf{r}'') = & 2 \sum_i^{\text{occ}} \sum_j^{\text{unocc}} \frac{\varphi_j^*(\mathbf{r}') \varphi_j(\mathbf{r}) \varphi_i^*(\mathbf{r}) \varphi_i(\mathbf{r}'')}{\epsilon_i - \epsilon_j} \\ & + 2 \sum_i^{\text{occ}} \sum_j^{\text{unocc}} \frac{\varphi_i^*(\mathbf{r}') \varphi_i(\mathbf{r}) \varphi_j^*(\mathbf{r}) \varphi_j(\mathbf{r}'')}{\epsilon_i - \epsilon_j}. \end{aligned} \quad (10)$$

Both χ_s and Λ_s contain summations over occupied and unoccupied states.

The OEP equation allows us to interpret the optimal local exchange potential as the potential that makes the perturbation ($V_x - v_x$), i.e. the perturbation that turns the KS equation into the HF equation, produce a vanishing first order density response [65, 66].

The theory presented above can readily be generalized to other approximations based on nonlocal exchange such as hybrid functionals [29, 35]. In the present work, we have used the PBE0 functional, which mixes in a fraction $\alpha = 0.25$ of nonlocal exact exchange in the PBE functional. Contrary to the HF method, electronic correlation is present but remains described at the PBE level.

A direct numerical solution of the OEP equation requires the construction of the response functions χ_s and Λ_s , and the subsequent inversion of χ_s . This procedure has been shown to work well on small systems but can give rise to numerical instabilities, in particular when Gaussian basis sets are used [39–41]. With large basis sets, such as plane waves, it can instead be computationally demanding as it requires the summation over all unoccupied states and the manipulation of large matrices [52].

An iterative approach that avoids some of these problems was developed by Kümmel and Perdew [50, 51] and generalized to the plane-wave and pseudopotential framework by Nguyen et al [52, 67]. The basic idea is to exploit the fact that the left and right hand sides of the OEP equation are linear density responses, $\delta n[v_x]$ and $\delta n[V_x]$, of the potentials v_x and V_x , respectively. These responses can be calculated within Density Functional Perturbation Theory (DFPT), a framework developed for the calculation of phonon modes [68]. For a given trial potential v_x^i , the two density responses will differ but their difference

$$\Delta n^i(\mathbf{r}) = \delta n[v_x^i](\mathbf{r}) - \delta n[V_x](\mathbf{r}) \quad (11)$$

can be used to update v_x according to

$$v_x^{i+1}(\mathbf{r}) = v_x^0(\mathbf{r}) + \sum_{m=1}^i \beta_m \Delta n^m(\mathbf{r}), \quad (12)$$

where v_x^0 is the initial trial potential. In each iteration, the coefficients β_m are determined by minimizing the integral of $|\Delta n^{i+1}|$ and convergence is achieved when this value reaches a given threshold. The converged exchange potential is then used to update v_{eff} and the KS equation is solved non-self-consistently to generate a new set of orbitals that are used for solving the OEP equation another time. This cyclic procedure continues until the electronic density is found converged to a given threshold. An extension of this scheme to hybrid functionals and solids can be found in Refs. 35 and 69.

III. ANALYTICAL FORCES WITH OEP

To understand the stability of a system, its set of nuclear forces needs to be computed. For a fixed configuration of the nuclei, each force \mathbf{F}_I describes the variation of the ground-state energy with respect to the position \mathbf{R}_I of a given nucleus I

$$\mathbf{F}_I = - \frac{\partial E_{\text{tot}}^{\mathbf{R}}}{\partial \mathbf{R}_I}. \quad (13)$$

Following the notation in Ref. 70, we denote the set of nuclear positions as $\mathbf{R} = \{\mathbf{R}_I\}$. At equilibrium geometry, the force exerted on each nucleus is zero. Calculating the second derivative of $E_{\text{tot}}^{\mathbf{R}}$ with respect to \mathbf{R}_I then yields interatomic force constants, which are necessary quantities for computing harmonic vibrational frequencies [71].

The derivative in Eq. (13) can be evaluated using the Hellmann-Feynman theorem (HFT) [72, 73], which states that due to the stationary property of the total energy, it is sufficient to consider the explicit dependence on external parameters, here the nuclear positions. The HFT is valid in DFT and with the OEP method.

The total force becomes a sum of two components

$$\mathbf{F}_I = \mathbf{F}_I^{\text{NN}} + \mathbf{F}_I^{\text{ext}}. \quad (14)$$

The first term is the derivative of the nuclear-nuclear potential energy

$$\mathbf{F}_I^{\text{NN}} = - \frac{\partial E_{\text{NN}}^{\mathbf{R}}}{\partial \mathbf{R}_I} = - \frac{\partial}{\partial \mathbf{R}_I} \sum_{J \neq I} \frac{Z_I Z_J}{|\mathbf{R}_I - \mathbf{R}_J|}, \quad (15)$$

where Z_I is the charge of nucleus I . The second term has its origin in the interaction between the nuclei and the electrons

$$\mathbf{F}_I^{\text{ext}} = - \int n^{\mathbf{R}}(\mathbf{r}) \frac{\partial v_{\text{ext}}^{\mathbf{R}}(\mathbf{r})}{\partial \mathbf{R}_I} d\mathbf{r}, \quad (16)$$

where

$$v_{\text{ext}}^{\mathbf{R}}(\mathbf{r}) = \sum_I \frac{Z_I}{|\mathbf{R}_I - \mathbf{r}|}. \quad (17)$$

The calculation of $\mathbf{F}_I^{\text{ext}}$ requires the knowledge of the electronic density $n^{\mathbf{R}}(\mathbf{r})$, obtained by performing a self-consistent calculation at fixed nuclear geometry \mathbf{R} .

A. Nonlocal pseudopotentials

The force equations presented so far are valid in the context of all-electron calculations. However, in practice, pseudopotentials are often used to reduce the computational cost. In this approach, the core electrons are frozen and described by an effective interaction. In general, the pseudopotential is separated into two contributions [74, 75]

$$v_{\text{ext}}(\mathbf{r}, \mathbf{r}') = v_{\text{L}}(\mathbf{r})\delta(\mathbf{r}, \mathbf{r}') + v_{\text{NL}}(\mathbf{r}, \mathbf{r}'). \quad (18)$$

The first term is fully local while the second is non-local both in the radial and the angular momentum dependence. This nonlocal contribution is written as a sum of projectors, which are functions of the spherical harmonics. The action of projectors is short-ranged as they are only defined within the core radius, i.e., the cutoff region [76–78]. Such a separable form for the pseudopotential allows an accurate reproduction of the scattering properties of the all-electron external potential. It also crucially improves the computational efficiency with respect to the size of the plane wave basis set used.

A nonlocal external potential does not pose any problem for functionals depending explicitly on the density or the gradient of the density because the total energy is not only stationary with respect to the density, but also with respect to variations of the KS density matrix. The expression for the external force term, Eq. (16), then only needs to be modified by replacing the density with the density matrix

$$\mathbf{F}_I^{\text{ext}} = - \int \gamma^{\mathbf{R}}(\mathbf{r}, \mathbf{r}') \frac{\partial v_{\text{ext}}^{\mathbf{R}}(\mathbf{r}, \mathbf{r}')}{\partial \mathbf{R}_I} d\mathbf{r} d\mathbf{r}'. \quad (19)$$

However, the total energy with OEP functionals is not stationary with respect to the KS density matrix, but with respect to the effective local potential. This difference leads to an extra term in the expression for the OEP total force. To derive this term, let us look at the EXX total energy at fixed nuclear positions \mathbf{R}

$$\begin{aligned} E_{\text{tot}}^{\mathbf{R}, \text{EXX}} &= 2 \sum_i^{\text{occ}} \epsilon_i^{\mathbf{R}} - \int v_{\text{Hxc}}^{\mathbf{R}}(\mathbf{r}) n^{\mathbf{R}}(\mathbf{r}) d\mathbf{r} \\ &+ \frac{1}{2} \int n^{\mathbf{R}}(\mathbf{r}) v(\mathbf{r} - \mathbf{r}') n^{\mathbf{R}}(\mathbf{r}') d\mathbf{r} d\mathbf{r}' \\ &- \frac{1}{4} \int \gamma^{\mathbf{R}}(\mathbf{r}, \mathbf{r}') v(\mathbf{r} - \mathbf{r}') \gamma^{\mathbf{R}}(\mathbf{r}', \mathbf{r}) d\mathbf{r} d\mathbf{r}' \\ &+ E_{\text{NN}}^{\mathbf{R}}, \end{aligned} \quad (20)$$

and take the derivative with respect to \mathbf{R}_I . We get straightforwardly

$$\mathbf{F}_I^{\text{EXX}} = \mathbf{F}_I^{\text{NN}} + \mathbf{F}_I^{\text{ext}} + \Delta \mathbf{F}_I^{\text{EXX}}, \quad (21)$$

where $\mathbf{F}_I^{\text{ext}}$ is given by Eq. (19) and

$$\begin{aligned} \Delta \mathbf{F}_I^{\text{EXX}} &= - \int v_{\text{x}}^{\mathbf{R}}(\mathbf{r}) \frac{\partial n^{\mathbf{R}}(\mathbf{r})}{\partial \mathbf{R}_I} d\mathbf{r} \\ &+ \int V_{\text{x}}^{\mathbf{R}}(\mathbf{r}, \mathbf{r}') \frac{\partial \gamma^{\mathbf{R}}(\mathbf{r}, \mathbf{r}')}{\partial \mathbf{R}_I} d\mathbf{r} d\mathbf{r}'. \end{aligned} \quad (22)$$

If the external potential was fully local, $\Delta \mathbf{F}_I^{\text{EXX}}$ would vanish at self-consistency thanks to the OEP equation, Eq. (8), being fulfilled. However, when the derivative of $n^{\mathbf{R}}$ and $\gamma^{\mathbf{R}}$ is taken via a nonlocal potential, the two terms in Eq. (22) are not guaranteed to cancel. To see this, let us look more closely at the derivative of the density with respect to the nuclear positions

$$\begin{aligned} \frac{\delta n^{\mathbf{R}}(\mathbf{r})}{\delta v_{\text{eff}}^{\mathbf{R}}(\mathbf{r}', \mathbf{r}'')} \frac{\partial v_{\text{eff}}^{\mathbf{R}}(\mathbf{r}', \mathbf{r}'')}{\partial \mathbf{R}_I} &= \frac{\delta n^{\mathbf{R}}(\mathbf{r})}{\delta v_{\text{eff}}^{\mathbf{R}}(\mathbf{r}', \mathbf{r}'')} \times \\ &\left[\left(\frac{\partial v_{\text{L}}^{\mathbf{R}}(\mathbf{r}')}{\partial \mathbf{R}_I} + \frac{\partial v_{\text{Hxc}}^{\mathbf{R}}(\mathbf{r}')}{\partial \mathbf{R}_I} \right) \delta(\mathbf{r}', \mathbf{r}'') + \frac{\partial v_{\text{NL}}^{\mathbf{R}}(\mathbf{r}', \mathbf{r}'')}{\partial \mathbf{R}_I} \right]. \end{aligned} \quad (23)$$

The derivatives via the local potentials ($v_{\text{L}}^{\mathbf{R}}$ and $v_{\text{Hxc}}^{\mathbf{R}}$) involve the standard non-interacting KS density response function (see Eq. (9)). Therefore, when the OEP equation is fulfilled, they cancel exactly the corresponding contributions coming from the derivative of the density matrix with respect to the nuclear positions in Eq. (22). However, the derivative via the nonlocal potential ($v_{\text{NL}}^{\mathbf{R}}$) requires the three-argument non-interacting KS density response function. The OEP equation can thus not be used and we are left with the following extra force term to evaluate

$$\begin{aligned} \Delta \mathbf{F}_I^{\text{EXX}} &= - \int v_{\text{x}}^{\mathbf{R}}(\mathbf{r}) \frac{\delta n^{\mathbf{R}}(\mathbf{r})}{\delta v_{\text{eff}}^{\mathbf{R}}(\mathbf{r}', \mathbf{r}'')} \frac{\partial v_{\text{NL}}^{\mathbf{R}}(\mathbf{r}', \mathbf{r}'')}{\partial \mathbf{R}_I} d\mathbf{r} d\mathbf{r}' d\mathbf{r}'' \\ &+ \int V_{\text{x}}^{\mathbf{R}}(\mathbf{r}, \mathbf{r}') \frac{\delta \gamma^{\mathbf{R}}(\mathbf{r}, \mathbf{r}')}{\delta v_{\text{eff}}^{\mathbf{R}}(\mathbf{r}'', \mathbf{r}''')} \frac{\partial v_{\text{NL}}^{\mathbf{R}}(\mathbf{r}'', \mathbf{r}''')}{\partial \mathbf{R}_I} d\mathbf{r} d\mathbf{r}' d\mathbf{r}'' d\mathbf{r}'''. \end{aligned} \quad (24)$$

We note that, since the nonlocal part of the external potential is fixed in the self-consistent procedure, i.e., it does not depend on the orbitals, only the bare responses are needed. The computational cost of this extra force term, calculated for the complete set of ions, is, therefore, estimated to be similar to a single iteration of the self-consistent procedure.

The extra force term due to the nonlocal pseudopotential will appear for any functional based on the OEP approach. In this work we have focused on hybrid functionals and norm-conserving pseudopotentials, and implemented Eq. (24) at the end of the self-consistent cycle. This was done within a modified version of the OEP implementation in the ACFDT (Adiabatic Connection Fluctuation Dissipation Theorem) package of the QUANTUM ESPRESSO distribution [35, 52, 67, 79]. In order to evaluate the change in the KS orbitals with respect to variations in the ionic positions, we have imported and adapted routines based on DFPT from the PHonon package. The internuclear and external force terms (Eqs. (15) and (19)) are general and both already implemented in the PWscf package.

With the knowledge of analytical forces, the design of a structural optimization tool for the OEP method can be devised. We have completed it by adapting the existing Broyden-Fletcher-Goldfarb-Shanno algorithm [80–83] implemented within PWscf.

B. Numerical test

As discussed in section II, the OEP self-consistent procedure runs two intertwined parts. One solves the Kohn-Sham equation non-self-consistently to retrieve the electronic density and the corresponding KS orbitals of the ground-state, while the other solves the OEP equation iteratively to generate the local EXX potential. The whole procedure is initialized with a good starting guess for the KS potential. We have found the PBE approximation to be a convenient choice in this regard. In addition to the plane wave basis set cutoff, there are two parameters that control the accuracy of the final results. The accuracy of the iterative solution to the OEP equation is determined by setting a threshold for $\int |\Delta n|$ (see Eq. (11)), and the accuracy of the self-consistent OEP potential is determined by setting a threshold for the difference in KS densities in-between successive cycles.

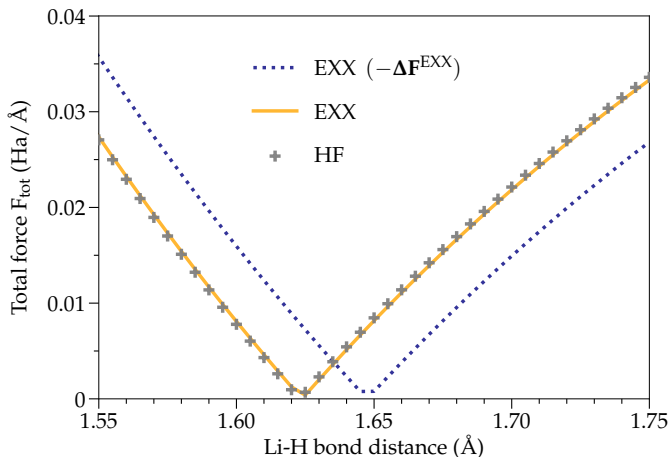


Figure 1. Change in the analytical total force F_{tot} (defined in Eq. (25)) of the LiH molecule upon variations of its intramolecular bond distance. The HF method is compared to EXX with and without the extra force term in Eq. (24).

In principle, one should use pseudopotentials optimized for the specific functional used [53]. However, since our objectives are to study the numerical precision and to compare OEP to generalized KS calculations we have settled for PBE optimized norm-conserving Vanderbilt (ONCV) pseudopotentials [84]. Independently of the functional used to optimize the pseudopotential they will, in general, contain nonlocal projectors and the extra OEP force term in Eq. (24) is necessary to include.

We first tested our implementation of the OEP forces on a simple system, the LiH molecule. We used a simulation cell of 20 Bohr and a plane-wave basis set with a kinetic energy cutoff of 80 Ry. The quantity we are interested in is the so-called "total force", which is defined

as

$$F_{\text{tot}} = \sqrt{\sum_{I=1}^M \sum_{\alpha=1}^3 (F_I^\alpha)^2} \quad (25)$$

where the α -index runs over the Cartesian components of the force on each of the M ions. The quantity F_{tot} is a positive-definite scalar able to describe the global behaviour of the system. Its value decreases upon approaching an energy minimum, and is zero at equilibrium.

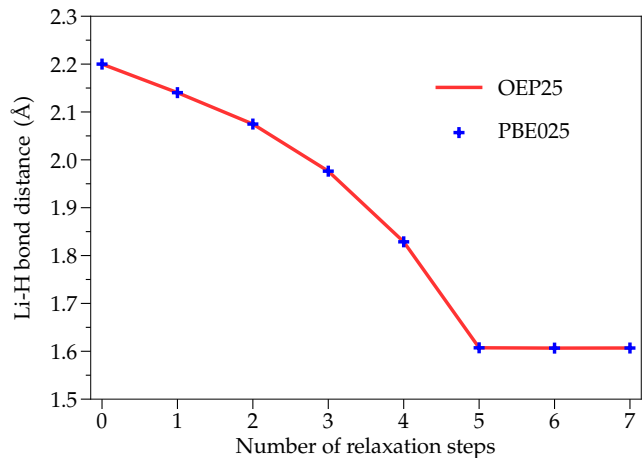


Figure 2. Evolution of the intramolecular bond distance of the LiH molecule after each iteration of the geometry relaxation procedure. The nonlocal PBE025 functional is compared to the local OEP25.

In Fig. 1, the total force is plotted as a function of the Li-H intramolecular bond distance within the HF and EXX approximations. The EXX calculations have been performed with and without the inclusion of the extra OEP force term, ΔF^{EXX} . Without this term, EXX predicts an equilibrium bond distance at 1.645 Å as compared to 1.625 Å for HF. The difference of 0.020 Å corresponds to a difference in F_{tot} of 0.008 Ha/Å. On the other hand, if we looked at the total EXX energy as a function of bond distance, we would find the same geometry at equilibrium as with HF. This inconsistency can be explained by the missing OEP force term, previously identified. Including it in the calculation of F_{tot} gives a good agreement between the EXX and HF total forces on the LiH molecule. Given that the importance of including nonlocal projectors in pseudopotentials increases with the number of electrons, we expect that ΔF^{EXX} will become even more important for heavier elements.

Having verified that the OEP forces come out accurately, we then optimized the geometry of the LiH molecule. Since the HF approximation is not expected to give a good equilibrium geometry, we used PBE0 with 25% of exact exchange (PBE025). We compared the fully nonlocal PBE025, already implemented, to the corresponding local OEP version, which we call OEP25. In

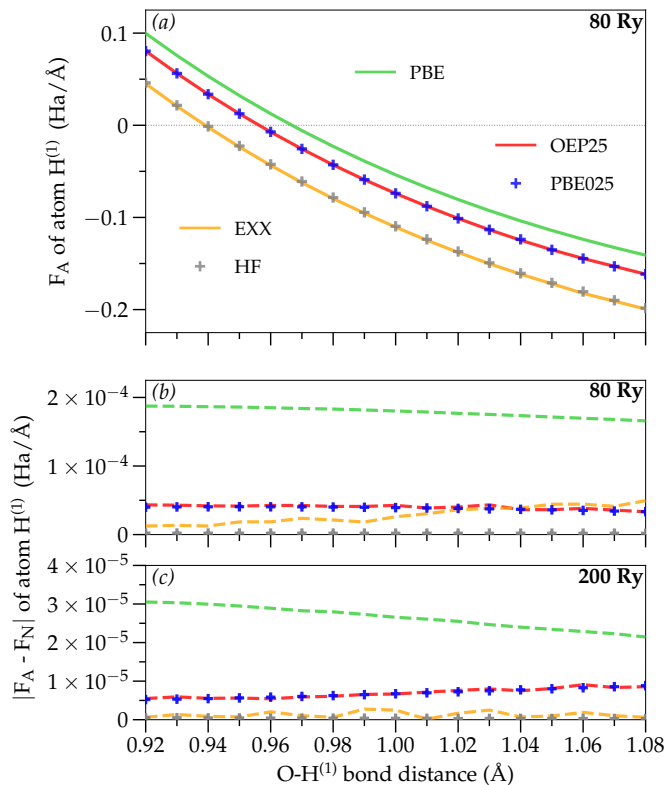


Figure 3. (a) Change in the analytical force F_A exerted on one of the hydrogen atoms of the H_2O molecule along the bond it forms with the O atom, according to different approximations. The corresponding numerical force F_N is not plotted as it is indistinguishable from F_A on the scale of the figure. (b) Absolute difference between F_A and F_N forces at fixed cutoff of 80 Ry and (c) 200 Ry.

Fig. 2, we see that starting from a Li-H bond length of 2.200 Å, the convergence of the geometry with OEP25 follows the same pattern as PBE025. The relaxation steps are similar, with both methods returning, after only five iterations, the same intramolecular bond distance of 1.607 Å.

We will now present a more comprehensive study of the accuracy of OEP forces by comparing the analytical force, F_A , as obtained from Eq. (21), with the numerical force, F_N , calculated by finite difference, using the five-point stencil formula with a step size of 0.01 Å. Given that energies converge faster than forces thanks to error cancellation, numerical forces also converge faster than analytical ones. Indeed, F_A is calculated by omitting certain contributions that are zero only at perfect self-consistency. The absolute difference $|F_A - F_N|$ can therefore be viewed as an estimation of the error on the analytical forces calculated and the quality of the self-consistent procedure. We started by studying the water molecule H_2O (see Fig. 3) using five different approximations: PBE, HF, EXX, PBE025, and OEP25. All data have been obtained using a simulation cell of 25 Bohr, and results for 80 Ry and 200 Ry plane-wave cutoff are

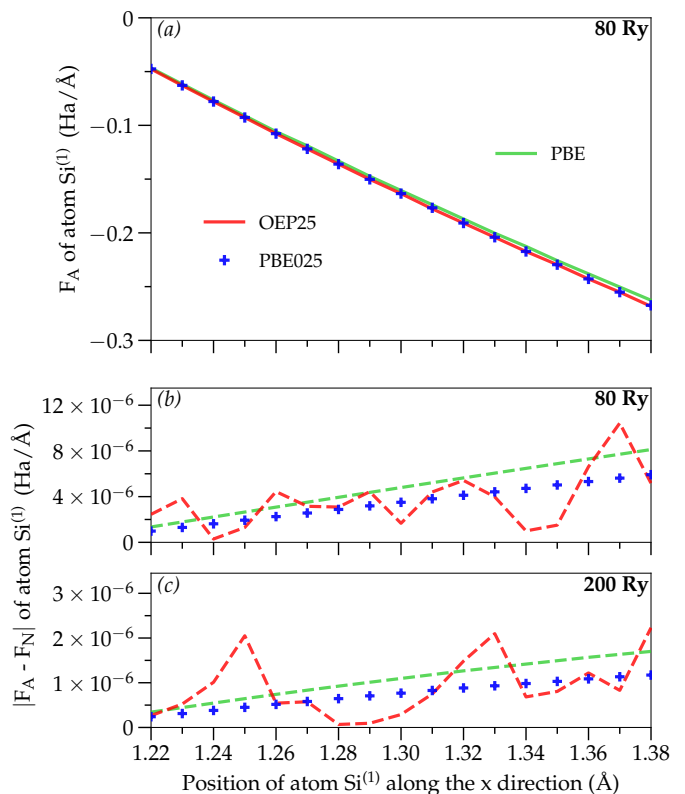


Figure 4. (a) Change in the analytical force F_A exerted on one of the silicon ion of the α - SiO_2 quartz phase upon variations of its position along the Cartesian x-axis, according to different approximations and at a plane-wave cutoff of 80 Ry. The corresponding numerical force F_N is not plotted as it is indistinguishable from F_A on the scale of the figure. (b) Absolute difference between F_A and F_N forces at fixed cutoff of 80 Ry and (c) 200 Ry.

compared. The threshold on the energy convergence of PBE, HF, and PBE025 was set to lowest possible value to ensure high accuracy of the numerical forces. The same was done for the two different thresholds used by EXX and OEP25 (see Sec. II). Regarding the atomic structure, the angle between the two O-H bonds has been fixed to 104.3°. Only the O-H⁽¹⁾ bond distance is varied while the length of O-H⁽²⁾ is set to 0.97 Å. These parameters define a geometry for the water molecule that is close to the PBE equilibrium geometry. By performing several test calculations at different geometries, we found that the choice of starting geometry does not impact the results we obtained on H_2O .

In Fig. 3(a), we plot the analytical force on atom $H^{(1)}$ along the O-H⁽¹⁾ bond distance as the bond is stretched. A smooth behaviour is observed for every method. Similarly to LiH, the effect of using a local OEP potential as an approximation to the nonlocal Fock exchange potential appears very small for both HF and PBE025. In Fig. 3(b), the difference between analytical and numerical forces is calculated at a cutoff of 80 Ry. For every

Table I. Structure parameters and vibration frequencies of the H₂O molecule calculated at equilibrium geometry with various methods. The O-H bond distance and the H-O-H bond angle are given. The frequencies have been calculated for the infrared active modes in-plane scissoring $\delta_{\text{H-O-H}}$, symmetric stretching $\nu_{\text{O-H}}^s$, and asymmetric stretching $\nu_{\text{O-H}}^{as}$. Results obtained in the literature with CCSD(T)/TZ(2df,2pd) [85] as well as experimental results [86] are also presented for reference.

	d(O-H) (Å)	$\Theta(\text{H-O-H})$ (°)	$\delta_{\text{H-O-H}}$ (cm ⁻¹)	$\nu_{\text{O-H}}^s$ (cm ⁻¹)	$\nu_{\text{O-H}}^{as}$ (cm ⁻¹)
PBE	0.9668	104.38	1597	3703	3816
PBE025	0.9558	104.91	1640	3857	3971
OEP25	0.9558	104.91	1639	3858	3972
HF	0.9385	106.06	1760	4113	4221
EXX	0.9380	106.17	1757	4123	4233
CCSD(T) [85]	0.9594	104.2	1650	3835	3944
Harmonic expt [86]	0.9572	104.52	1649	3832	3943
Anharmonic expt [86]	0.9572	104.52	1595	3657	3756

method, the scale of the error on F_A is found to be relatively small. The performance of the hybrid PBE025 functional is one order of magnitude better than PBE, and three orders of magnitude better with HF. If we now analyze the performance of the OEP methods, we notice that OEP25 produces a similar error to PBE025, which on average is about 4×10^{-5} Ha/Å at 80 Ry. On the other hand, EXX fails to deliver the exceptionally small error seen with HF. While HF returns force differences of the order of 10^{-7} Ha/Å, EXX results are closer in magnitude to PBE025 and OEP25. The difference observed between EXX and HF is probably related to the threshold used to solve the OEP equation. In Fig. 3(c) we present the same curves as in Fig. 3(b) but with a higher plane-wave cutoff of 200 Ry. An improvement of roughly one order of magnitude is seen in the error profile of all methods except HF, for which the error was already very small. The enhanced performance of the EXX approximation suggests that, for a given threshold used to solve the OEP equation, a higher plane-wave cutoff helps to improve the accuracy of the EXX potential. For the OEP methods, the extra source of error related to the evaluation of the local KS potential via the OEP equation seems to have a small impact. This is evident from the good agreement observed between OEP25 and PBE025 in Figs. 3(b) and 3(c). Only small irregularities in the error of the force can be seen with OEP25.

To investigate whether the high accuracy we observe on molecules also extends to solids, we have performed the same analysis of forces on the α -quartz phase of SiO₂. For this solid that belongs to the P3₂₂₁ space group, cell parameters and atomic positions have first been relaxed at the PBE level using a uniform 333 Monkhorst-Pack grid of \mathbf{k} points and a cutoff of 80 Ry. On the optimized structure, one of the silicon ions has then been displaced away from its equilibrium position along the Cartesian x-axis, and the change in the force exerted on this ion has been monitored using PBE, PBE025 and OEP25 at 80 Ry and 200 Ry. The data obtained are presented in

Fig. 4.

Similarly to the conclusions drawn from Fig. 3, we find on silica that PBE025 performs better than PBE at fixed planewave cutoff. The overall error on F_A forces is, however, smaller on SiO₂ as compared to H₂O. This renders the irregularities in the error profile of OEP25 more apparent, despite their amplitudes being very small, about 5×10^{-6} Ha/Å at 80 Ry. Given the magnitude of the force exerted on ion Si⁽¹⁾ in Fig. 4(a), the errors observed here are not expected to be of practical importance. As already noticed on H₂O, using a larger cutoff leads to a decrease of the error in analytical forces for all methods. The OEP25 irregularities are also dampened, reducing from 5×10^{-6} Ha/Å at 80 Ry to 2×10^{-6} Ha/Å at 200 Ry. The different results obtained on SiO₂ confirm a good accuracy of the OEP forces for periodic solids. We have been able to identify two main sources of errors in the analytical forces. The first error is method dependent. Different functionals may need different cutoffs to be fully converged. The second error is specific to the OEP method and is related to the accuracy of the local potential generated from the iterative solution of the OEP equation. Both of these errors can be reduced by increasing the plane-wave cutoff and by improving the convergence thresholds of the OEP and KS equations.

IV. APPLICATIONS

Given the high accuracy seen in the previous section, the calculated OEP forces can be exploited to compute vibrational frequencies. In this section, we will calculate the OEP vibrational frequencies of different molecular and solid state systems, and compare them to the ones predicted by the corresponding methods that use a non-local exchange potential.

The three systems investigated are the water molecule H₂O, diamond, and the α -quartz phase of SiO₂. For H₂O, we used the same functionals as tested in Sec. III,

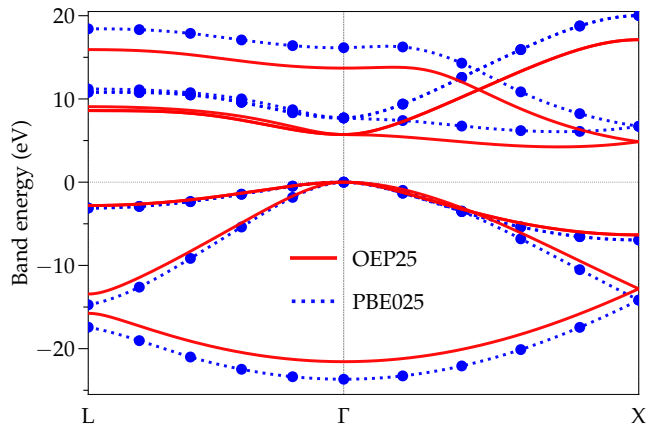


Figure 5. Band structure plot of diamond obtained along the high symmetry path L - Γ - X. Data have been obtained using PBE025 and OEP25. The PBE025 bands have been spline-interpolated between the dots.

i.e. PBE, HF, EXX, PBE025, and OEP25. For diamond and SiO₂, only PBE, PBE025 and OEP25 have been used. For each functional we first relaxed the structure. The vibration modes were subsequently determined using the Phonopy Python package [87, 88]. Considering the atomic positions and the existing symmetries in the system, this code is able to generate several relevant supercell configurations through slight displacement of the elements. After computation of the analytical forces of each supercell, the existing vibration modes in the system can be predicted by Phonopy and their frequency calculated by finite difference of the forces using the central derivative formula.

A. H₂O

The O-H bond distance $d(\text{O-H})$, the bond angle $\Theta(\text{H-O-H})$, and the vibrational frequencies of the infrared active modes of H₂O are presented in Table I. The data have been obtained using a simulation box size of 25 Bohr and a plane-wave cutoff of 80 Ry. The accuracy achieved at the end of the optimization procedure is excellent for all approximations. It has been possible to converge the O-H bond distance below 1×10^{-4} Å, the bond angle below 1×10^{-2} degree, and the vibrational frequencies below 1 cm^{-1} . We also tried increasing the cutoff from 80 to 200 Ry without noticing any changes in the results. This confirms that the errors in the forces noted at 80 Ry in Sec. III are sufficiently small to be of no relevance for an accurate determination of equilibrium geometries and vibrational frequencies.

If we compare the structural parameters from each method, we see that the equilibrium geometry predicted by OEP25 is consistent with that of PBE025. The good agreement between these two methods also extends to the vibrational frequencies, with PBE025 and OEP25 re-

turning similar values for the three infrared active modes, namely the in-plane scissoring $\delta_{\text{H-O-H}}$, the symmetric stretching $\nu_{\text{O-H}}^s$, and the asymmetric stretching $\nu_{\text{O-H}}^{as}$. On the other hand, small differences can be observed in the structural parameters obtained by the EXX and HF methods. Although very close in geometry, the changes in the O-H bond length and bond angle are sufficient to affect the vibrational frequencies. Compared to HF, EXX returns a lower frequency for the deformation mode, but higher for the two elongation modes. This change is consistent with the evolution of the structural parameters between the two methods as EXX predicts more rigid bonds and a looser angle than HF. The evolution of the structural parameters between EXX and its non-local exchange counterpart method HF also agrees with the results presented by Wu et al. [62]. It confirms that, despite including a maximal fraction of local OEP exact exchange, the EXX method is able to mimic well HF performance.

Compared to reference CCSD(T)/TZ(2df,2pd) [85] and harmonic experimental [86] data, PBE025 and OEP25 are the only two methods returning appropriate structural and vibrational properties for the isolated water molecule.

B. Diamond

Diamond crystallizes in the Fd-3m space group. Thanks to the high symmetry, the atomic positions are fixed within the unit cell. Only the lattice parameter a is left to vary in order to identify the optimized unit cell. We have identified the suitable cell dimensions by monitoring the change of the total energy upon variations of the lattice parameter a . The values of 6.700 Bohr for both OEP25 and PBE025, and 6.742 Bohr for PBE are optimal.

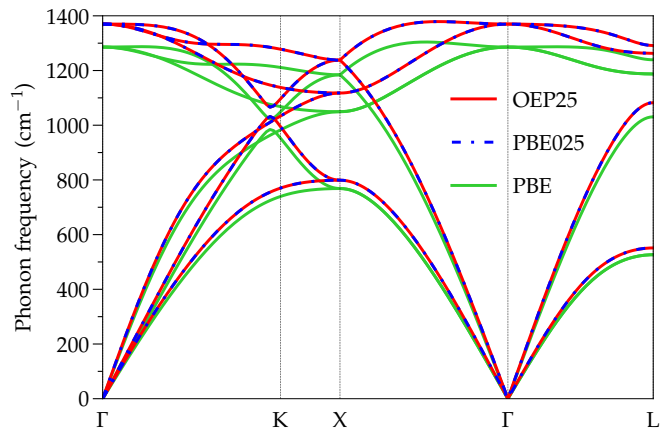


Figure 6. Phonon dispersion of diamond. The nonlocal PBE025 functional is compared to its local OEP25 counterpart and to PBE.

Table II. Structural parameters of α -SiO₂ according to different functionals. The internal parameters x , y , and z given describe the position of oxygen and silicon ions within the unit cell. The Si-O bond distances, the Si-O-Si bond angle and the O-Si-O bond angles are also given. For every methods considered, experimental unit cell parameters have been used ($a = 4.916$ Å, $c = 5.405$ Å) [89].

	PBE	PBE025	OEP25	Expt [89]
$x(\text{Si})$	0.4685	0.4727	0.4727	0.4697
$x(\text{O})$	0.4120	0.4147	0.4148	0.4135
$y(\text{O})$	0.2694	0.2623	0.2623	0.2669
$z(\text{O})$	0.1172	0.1235	0.1235	0.1191
$d(\text{Si-O})$ (Å)	1.612	1.599	1.599	1.605
	1.617	1.603	1.603	1.614
$\Theta(\text{Si-O-Si})$ (°)	142.7	145.3	145.3	143.7
$\Theta(\text{O-Si-O})$ (°)	108.7	108.9	108.9	108.8
	108.7	108.9	108.9	109.0
	109.1	109.2	109.2	109.2
	110.8	110.4	110.4	110.5

We first calculated the electronic band structure along the L - Γ - X high symmetry path within PBE025 and OEP25 (see Fig. 5). The OEP25 bands are easy to generate using post-processing tools since the local exchange potential is \mathbf{k} -independent. For PBE025 we only have the band energies on the \mathbf{k} -point grid used in the self-consistent calculation. The bands have, therefore, been spline-interpolated between these points. The band structures are clearly different in the two approximations. The first conduction band is shifted by approximately 2 eV in PBE025. This difference is expected and related to the derivative discontinuity within the OEP method [32, 33]. Adding the derivative discontinuity correction to the OEP25 result returns a gap in very good agreement with PBE025, with an energy difference of 0.02 eV.

We calculated the phonon dispersion along a high symmetry path in the Brillouin Zone with Phonopy using a single $2 \times 2 \times 2$ supercell containing 64 carbon atoms. A uniform 222 Monkhorst-Pack grid of \mathbf{k} points and a plane wave cutoff of 100 Ry have been employed. The results are presented in Fig. 6. Despite the use of the frozen phonon approach, our PBE results agree well with the data presented by Mounet et al. [90] using DFPT. We also notice a very good agreement between the PBE025 and OEP25 frequencies. As expected, both methods return higher frequencies than PBE because the effect of exact exchange is well known to strengthen bonds. This case study proves that accurate phonons can be calculated using the OEP method.

C. SiO₂

The last system we considered is the α -quartz phase of SiO₂. Unlike diamond, α -quartz silica has polar bonds. Therefore, correct phonons can only be obtained if the LO-TO splitting is explicitly calculated. To evaluate the LO-TO splitting, knowledge of the dielectric tensor and Born effective charges of all symmetry-inequivalent ions within the unit cell is required [70, 92]. However, since our present objective is to compare the performance of the OEP25 functional with respect to PBE025, we have neglected the LO-TO splitting correction when computing the phonon modes of SiO₂.

For this study, we have used experimental unit cell parameters [89] and then relaxed the atomic positions for each functional. We have used a uniform 333 Monkhorst-Pack dense grid of \mathbf{k} points and a plane-wave cutoff of 100 Ry. The structural parameters are presented in Table II. The internal coordinates $x(\text{Si})$, $x(\text{O})$, $y(\text{O})$, and $z(\text{O})$ describe, along with the symmetries of the crystal, the position of each ion within the cell. Given the complexity of the SiO₂ unit cell, it is remarkable that PBE025 and OEP25 produce similar structural parameters. These two methods give tighter bonds and looser angles than PBE. On the other hand, experimental structure parameters appear to be located halfway between these methods.

We then calculated the phonon modes at the Γ -point by generating a total of nine different $1 \times 1 \times 1$ supercells with Phonopy. The list of phonon modes and their associated frequencies are presented in Table III. For each mode, we find an excellent agreement between PBE025 and OEP25. As expected, by including a fraction of

Table III. Phonon frequencies calculated at the Γ -point of α -SiO₂ on the relaxed structures presented in Table II for different functionals. Frequencies are given in cm⁻¹. While the acoustic sum rule is applied, the LO-TO splitting is only considered in experimental results [91]. Phonon frequencies affected by LO-TO splitting are underlined in the table.

	PBE	PBE025	OEP25	Expt [91]
E_u(TO1)	140	67	67	133
E_u(LO1)	<u>140</u>	<u>67</u>	<u>67</u>	133
A₁(1)	211	167	167	219
E_u(TO2)	263	242	242	269
E_u(LO2)	<u>263</u>	<u>242</u>	<u>242</u>	269
A₁(2)	351	354	354	358
A₂(TO1)	352	363	364	361
E_u(TO3)	386	388	388	394
E_u(LO3)	<u>386</u>	<u>388</u>	<u>388</u>	402
E_u(TO4)	442	446	447	453
E_u(LO4)	<u>442</u>	<u>446</u>	<u>447</u>	512
A₁(3)	452	453	453	469
A₂(TO2)	484	489	489	499
E_u(TO5)	677	696	696	698
E_u(LO5)	<u>677</u>	<u>696</u>	<u>696</u>	701
A₂(TO3)	756	782	783	778
E_u(TO6)	776	797	797	799
E_u(LO6)	<u>776</u>	<u>797</u>	<u>797</u>	812
E_u(TO7)	1042	1085	1085	1066
E_u(LO7)	<u>1042</u>	<u>1085</u>	<u>1085</u>	1227
A₂(TO4)	1050	1092	1093	1072
A₁(4)	1061	1101	1102	1082
E_u(TO8)	1133	1181	1182	1158
E_u(LO8)	<u>1133</u>	<u>1181</u>	<u>1182</u>	1155

exact exchange, the frequencies obtained are in general higher in energy than that of PBE. For the TO modes located over 1000 cm⁻¹, experimental frequencies are located halfway between PBE and PBE025/OEP25 results, which might indicate that the true fraction of exact exchange to include for PBE0 should actually be lower than the standard 25%. The comparison with experimental data also show for which LO modes a significant shift of the frequencies we calculated can be expected.

This comprehensive analysis on SiO₂ α -quartz confirms that our implementation of OEP forces can be used for accurate studies of complex systems.

V. CONCLUSIONS AND OUTLOOK

Achieving full self-consistency with orbital-dependent xc functionals requires the solution of the OEP equation. Although numerically challenging, the OEP represents a simplification over the use of nonlocal and energy-

dependent potentials. Being formulated within the KS-DFT framework, it is, for example, easy to combine the OEP with existing codes for excited state properties (e.g. *GW*) or lattice dynamics.

In this work, we have shown that OEP forces, within hybrid functionals, can be computed with a numerical accuracy similar to that obtained with commonly used functionals in DFT. However, we also showed that special care is needed when employing nonlocal pseudopotentials. Since the OEP is based on a constrained optimization, an extra force term needs to be added to the standard Hellmann-Feynman expression for the forces. We implemented this term within the ACFDT package of the QUANTUM ESPRESSO distribution, that already computes the OEP potential. This allowed us to calculate forces, relax geometries, and determine phonon frequencies for a number of molecules and solids. Our different studies show that the local OEP exchange potential is a good approximation to the nonlocal exchange potential, being able to produce almost identical equilibrium

structures and phonon frequencies.

The high numerical accuracy we have obtained with the OEP applied to hybrid functionals paves the way for determining the OEP forces also with more advanced functionals, such as those based on MBPT. Furthermore, our work provides a first step towards the calculation of phonon spectra and electron-phonon couplings within DFPT, using an advanced treatment of exchange and

correlation.

ACKNOWLEDGMENTS

The authors would like to thank Michele Casula and Lorenzo Paulatto for helpful discussions. The work was partially performed using HPC resources from GENCI-TGCC/CINES/IDRIS (Grant No. A0150914650).

-
- [1] P. Hohenberg and W. Kohn, Inhomogeneous Electron Gas, *Phys. Rev.* **136**, B864–B871 (1964).
- [2] W. Kohn and L. J. Sham, Self-Consistent Equations Including Exchange and Correlation Effects, *Phys. Rev.* **140**, A1133–A1138 (1965).
- [3] R. G. Parr and W. Yang, *Density-Functional Theory of Atoms and Molecules* (Oxford University Press, New York, 1989).
- [4] C. Fiolhais, F. Nogueira, and M. A. L. Marques, *A Primer in Density Functional Theory*, 1st ed., Vol. 620 (Springer Berlin, Heidelberg, 2003).
- [5] W. Kohn, A. D. Becke, and R. G. Parr, Density Functional Theory of Electronic Structure, *The Journal of Physical Chemistry* **100**, 12974–12980 (1996).
- [6] J. P. Perdew and K. Schmidt, Jacob’s ladder of density functional approximations for the exchange-correlation energy, *AIP Conference Proceedings* **577**, 1–20 (2001).
- [7] D. Rappoport, N. R. M. Crawford, F. Furche, and K. Burke, Which functional should I choose?, in *Computational Inorganic and Bioinorganic Chemistry*, edited by E. I. Solomon, R. B. King, and R. A. Scott (Wiley, Chichester. Hoboken: Wiley, John & Sons, Inc., 2009).
- [8] J. P. Perdew and A. Zunger, Self-interaction correction to density-functional approximations for many-electron systems, *Phys. Rev. B* **23**, 5048–5079 (1981).
- [9] A. D. Becke, Density-functional thermochemistry. III. The role of exact exchange, *The Journal of Chemical Physics* **98**, 5648–5652 (1993).
- [10] J. Heyd, G. E. Scuseria, and M. Ernzerhof, Hybrid functionals based on a screened Coulomb potential, *The Journal of Chemical Physics* **118**, 8207–8215 (2003).
- [11] X. Ren, P. Rinke, C. Joas, and M. Scheffler, Random-phase approximation and its applications in computational chemistry and materials science, *Journal of Materials Science* **47**, 7447–7471 (2012).
- [12] A. Seidl, A. Görling, P. Vogl, J. A. Majewski, and M. Levy, Generalized Kohn-Sham schemes and the band-gap problem, *Phys. Rev. B* **53**, 3764–3774 (1996).
- [13] R. Garrick, A. Natan, T. Gould, and L. Kronik, Exact Generalized Kohn-Sham Theory for Hybrid Functionals, *Phys. Rev. X* **10**, 021040 (2020).
- [14] T. Lebeda, T. Aschebrock, J. Sun, L. Leppert, and S. Kümmel, Right band gaps for the right reason at low computational cost with a meta-GGA, *Phys. Rev. Mater.* **7**, 093803 (2023).
- [15] J. Paier, M. Marsman, K. Hummer, G. Kresse, I. C. Gerber, and J. G. Ángyán, Screened hybrid density functionals applied to solids, *The Journal of Chemical Physics* **124**, 154709 (2006).
- [16] F. G. Eich and M. Hellgren, Derivative discontinuity and exchange-correlation potential of meta-GGAs in density-functional theory, *The Journal of Chemical Physics* **141**, 224107 (2014).
- [17] Z. Yang, H. Peng, J. Sun, and J. P. Perdew, More realistic band gaps from meta-generalized gradient approximations: Only in a generalized Kohn-Sham scheme, *Phys. Rev. B* **93**, 205205 (2016).
- [18] A. Klein, Perturbation Theory for an Infinite Medium of Fermions. II, *Phys. Rev.* **121**, 950–956 (1961).
- [19] N. E. Dahlen, R. van Leeuwen, and U. von Barth, Variational energy functionals of the Green function and of the density tested on molecules, *Phys. Rev. A* **73**, 012511 (2006).
- [20] M. Hellgren and U. von Barth, Correlation potential in density functional theory at the GWA level: Spherical atoms, *Phys. Rev. B* **76**, 075107 (2007).
- [21] B. Holm and U. von Barth, Fully self-consistent GW self-energy of the electron gas, *Phys. Rev. B* **57**, 2108–2117 (1998).
- [22] A. Stan, N. E. Dahlen, and R. Van Leeuwen, Fully self-consistent GW calculations for atoms and molecules, *Europhys. Lett.* **76**, 298–304 (2006).
- [23] F. Caruso, P. Rinke, X. Ren, M. Scheffler, and A. Rubio, Unified description of ground and excited states of finite systems: The self-consistent GW approach, *Phys. Rev. B* **86**, 081102(R) (2012).
- [24] M. Grumet, P. Liu, M. Kaltak, J. c. v. Klimeš, and G. Kresse, Beyond the quasiparticle approximation: Fully self-consistent GW calculations, *Phys. Rev. B* **98**, 155143 (2018).
- [25] R. T. Sharp and G. K. Horton, A Variational Approach to the Unipotential Many-Electron Problem, *Phys. Rev.* **90**, 317–317 (1953).

- [26] J. D. Talman and W. F. Shadwick, Optimized effective atomic central potential, *Phys. Rev. A* **14**, 36–40 (1976).
- [27] K. Aashamar, T. M. Luke, and J. D. Talman, Properties of single-term atomic states calculated in a variationally optimized-local-central-potential model, *Phys. Rev. A* **19**, 6–16 (1979).
- [28] J. B. Krieger, Y. Li, and G. J. Iafrate, Construction and application of an accurate local spin-polarized Kohn-Sham potential with integer discontinuity: Exchange-only theory, *Phys. Rev. A* **45**, 101–126 (1992).
- [29] J. Kim, K. Hong, S.-Y. Hwang, S. Ryu, S. Choi, and W. Y. Kim, Effects of the locality of a potential derived from hybrid density functionals on Kohn-Sham orbitals and excited states, *Phys. Chem. Chem. Phys.* **19**, 10177-10186 (2017).
- [30] C.-O. Almbladh and U. von Barth, Exact results for the charge and spin densities, exchange-correlation potentials, and density-functional eigenvalues, *Phys. Rev. B* **31**, 3231–3244 (1985).
- [31] E. J. Baerends, O. V. Gritsenko, and R. van Meer, The Kohn-Sham gap, the fundamental gap and the optical gap: the physical meaning of occupied and virtual Kohn-Sham orbital energies, *Phys. Chem. Chem. Phys.* **15**, 16408-16425 (2013).
- [32] Y. Li, J. B. Krieger, M. R. Norman, and G. J. Iafrate, Band-structure calculations of noble-gas and alkali halide solids using accurate Kohn-Sham potentials with self-interaction correction, *Phys. Rev. B* **44**, 10437–10443 (1991).
- [33] J. P. Perdew, Density functional theory and the band gap problem, *International Journal of Quantum Chemistry* **28**, 497-523 (1985).
- [34] J. P. Perdew, R. G. Parr, M. Levy, and J. L. Balduz, Density-Functional Theory for Fractional Particle Number: Derivative Discontinuities of the Energy, *Phys. Rev. Lett.* **49**, 1691–1694 (1982).
- [35] M. Hellgren, L. Baguet, M. Calandra, F. Mauri, and L. Wirtz, Electronic structure of TiSe_2 from a quasi-self-consistent G_0W_0 approach, *Phys. Rev. B* **103**, 075101 (2021).
- [36] Y. M. Niquet and X. Gonze, Band-gap energy in the random-phase approximation to density-functional theory, *Phys. Rev. B* **70**, 245115 (2004).
- [37] M. Grüning, A. Marini, and A. Rubio, Effect of spatial nonlocality on the density functional band gap, *Phys. Rev. B* **74**, 161103(R) (2006).
- [38] J. Klimeš and G. Kresse, Kohn-Sham band gaps and potentials of solids from the optimised effective potential method within the random phase approximation, *The Journal of Chemical Physics* **140**, 054516 (2014).
- [39] A. Görling, New KS Method for Molecules Based on an Exchange Charge Density Generating the Exact Local KS Exchange Potential, *Phys. Rev. Lett.* **83**, 5459–5462 (1999).
- [40] A. Heßelmann, A. W. Götz, F. Della Sala, and A. Görling, Numerically stable optimized effective potential method with balanced Gaussian basis sets, *The Journal of Chemical Physics* **127**, 054102 (2007).
- [41] E. Trushin and A. Görling, Numerically stable optimized effective potential method with standard Gaussian basis sets, *The Journal of Chemical Physics* **155**, 054109 (2021).
- [42] M. Städele, M. Moukara, J. A. Majewski, P. Vogl, and A. Görling, Exact exchange Kohn-Sham formalism applied to semiconductors, *Phys. Rev. B* **59**, 10031–10043 (1999).
- [43] H. Jiang and E. Engel, Second-order Kohn-Sham perturbation theory: Correlation potential for atoms in a cavity, *The Journal of Chemical Physics* **123**, 224102 (2005).
- [44] A. Makmal, S. Kümmel, and L. Kronik, Fully Numerical All-Electron Solutions of the Optimized Effective Potential Equation for Diatomic Molecules, *Journal of Chemical Theory and Computation* **5**, 1731-1740 (2009).
- [45] M. Hellgren and U. von Barth, Linear density response function within the time-dependent exact-exchange approximation, *Phys. Rev. B* **78**, 115107 (2008).
- [46] M. Hellgren and U. von Barth, Exact-exchange kernel of time-dependent density functional theory: Frequency dependence and photoabsorption spectra of atoms, *The Journal of Chemical Physics* **131**, 044110 (2009).
- [47] M. Hellgren and U. von Barth, Correlation energy functional and potential from time-dependent exact-exchange theory, *The Journal of Chemical Physics* **132**, 044101 (2010).
- [48] M. Hellgren and E. K. U. Gross, Discontinuous functional for linear-response time-dependent density-functional theory: The exact-exchange kernel and approximate forms, *Phys. Rev. A* **88**, 052507 (2013).
- [49] W. Yang and Q. Wu, Direct Method for Optimized Effective Potentials in Density-Functional Theory, *Phys. Rev. Lett.* **89**, 143002 (2002).
- [50] S. Kümmel and J. P. Perdew, Simple Iterative Construction of the Optimized Effective Potential for Orbital Functionals, Including Exact Exchange, *Phys. Rev. Lett.* **90**, 043004 (2003).
- [51] S. Kümmel and J. P. Perdew, Optimized effective potential made simple: Orbital functionals, orbital shifts, and the exact Kohn-Sham exchange potential, *Phys. Rev. B* **68**, 035103 (2003).
- [52] N. L. Nguyen, N. Colonna, and S. de Gironcoli, Ab initio self-consistent total-energy calculations within the EXX/RPA formalism, *Phys. Rev. B* **90**, 045138 (2014).
- [53] E. Engel, A. Höck, R. N. Schmid, R. M. Dreizler, and N. Chetty, Role of the core-valence interaction for pseudopotential calculations with exact exchange, *Phys. Rev. B* **64**, 125111 (2001).
- [54] S. Sharma, J. K. Dewhurst, and C. Ambrosch-Draxl,

- All-Electron Exact Exchange Treatment of Semiconductors: Effect of Core-Valence Interaction on Band-Gap and d -Band Position, *Phys. Rev. Lett.* **95**, 136402 (2005).
- [55] A. Makmal, R. Armiento, E. Engel, L. Kronik, and S. Kümmel, Examining the role of pseudopotentials in exact-exchange-based Kohn-Sham gaps, *Phys. Rev. B* **80**, 161204(R) (2009).
- [56] M. Betzinger, C. Friedrich, S. Blügel, and A. Görling, Local exact exchange potentials within the all-electron FLAPW method and a comparison with pseudopotential results, *Phys. Rev. B* **83**, 045105 (2011).
- [57] S. Kümmel and L. Kronik, Orbital-dependent density functionals: Theory and applications, *Rev. Mod. Phys.* **80**, 3–60 (2008).
- [58] E. Trushin and A. Görling, Assessment of quality and reliability of band structures from exact-exchange-only Kohn–Sham, hybrid, and GW methods, *The European Physical Journal B* **91**, 149 (2018).
- [59] E. Trushin, L. Fromm, and A. Görling, Assessment of the exact-exchange-only Kohn-Sham method for the calculation of band structures for transition metal oxide and metal halide perovskites, *Phys. Rev. B* **100**, 075205 (2019).
- [60] P. Rinke, A. Qteish, J. Neugebauer, C. Freysoldt, and M. Scheffler, Combining *GW* calculations with exact-exchange density-functional theory: an analysis of valence-band photoemission for compound semiconductors, *New J. Phys.* **7**, 126 (2005).
- [61] A. Qteish, P. Rinke, M. Scheffler, and J. Neugebauer, Exact-exchange-based quasiparticle energy calculations for the band gap, effective masses, and deformation potentials of ScN, *Phys. Rev. B* **74**, 245208 (2006).
- [62] Q. Wu, A. J. Cohen, and W. Yang, Analytic energy gradients of the optimized effective potential method, *The Journal of Chemical Physics* **123**, 134111 (2005).
- [63] A. Thierbach and A. Görling, Analytic energy gradients for the exact exchange Kohn–Sham method, *The Journal of Chemical Physics* **152**, 114113 (2020).
- [64] A. Thierbach and A. Görling, Analytic energy gradients for the self-consistent direct random phase approximation, *The Journal of Chemical Physics* **153**, 134113 (2020).
- [65] L. J. Sham and M. Schlüter, Density-Functional Theory of the Energy Gap, *Phys. Rev. Lett.* **51**, 1888–1891 (1983).
- [66] M. E. Casida, Generalization of the optimized-effective-potential model to include electron correlation: A variational derivation of the Sham-Schlüter equation for the exact exchange-correlation potential, *Phys. Rev. A* **51**, 2005–2013 (1995).
- [67] P. Giannozzi, O. Andreussi, T. Brumme, O. Bunau, M. B. Nardelli, M. Calandra, R. Car, C. Cavazzoni, D. Ceresoli, M. Cococcioni, N. Colonna, I. Carnimeo, A. D. Corso, S. de Gironcoli, P. Delugas, R. A. DiStasio, A. Ferretti, A. Floris, G. Fratesi, G. Fugallo, R. Gebauer, U. Gerstmann, F. Giustino, T. Gorni, J. Jia, M. Kawamura, H.-Y. Ko, A. Kokalj, E. Kucukbenli, M. Lazzeri, M. Marsili, N. Marzari, F. Mauri, N. L. Nguyen, H.-V. Nguyen, A. O. de-la Roza, L. Paulatto, S. Poncé, D. Rocca, R. Sabatini, B. Santra, M. Schlipf, A. P. Seitsonen, A. Smogunov, I. Timrov, T. Thonhauser, P. Umari, N. Vast, X. Wu, and S. Baroni, Advanced capabilities for materials modelling with Quantum ESPRESSO, *Journal of Physics: Condensed Matter* **29**, 465901 (2017).
- [68] S. Baroni, P. Giannozzi, and A. Testa, Green’s-function approach to linear response in solids, *Phys. Rev. Lett.* **58**, 1861–1864 (1987).
- [69] M. Hellgren and L. Baguet, Random phase approximation with exchange for an accurate description of crystalline polymorphism, *Phys. Rev. Res.* **3**, 033263 (2021).
- [70] S. Baroni, S. de Gironcoli, A. Dal Corso, and P. Giannozzi, Phonons and related crystal properties from density-functional perturbation theory, *Rev. Mod. Phys.* **73**, 515–562 (2001).
- [71] R. M. Pick, M. H. Cohen, and R. M. Martin, Microscopic Theory of Force Constants in the Adiabatic Approximation, *Phys. Rev. B* **1**, 910–920 (1970).
- [72] H. Hellman, Einführung in die Quantenchemie, Franz Deuticke, Leipzig **285** (1937).
- [73] R. P. Feynman, Forces in Molecules, *Phys. Rev.* **56**, 340–343 (1939).
- [74] D. R. Hamann, M. Schlüter, and C. Chiang, Norm-Conserving Pseudopotentials, *Phys. Rev. Lett.* **43**, 1494–1497 (1979).
- [75] R. M. Martin, *Electronic Structure: Basic Theory and Practical Methods* (Cambridge University Press, 2004).
- [76] L. Kleinman and D. M. Bylander, Efficacious Form for Model Pseudopotentials, *Phys. Rev. Lett.* **48**, 1425–1428 (1982).
- [77] P. E. Blöchl, Generalized separable potentials for electronic-structure calculations, *Phys. Rev. B* **41**, 5414–5416 (1990).
- [78] D. Vanderbilt, Soft self-consistent pseudopotentials in a generalized eigenvalue formalism, *Phys. Rev. B* **41**, 7892–7895 (1990).
- [79] H.-V. Nguyen and S. de Gironcoli, Efficient calculation of exact exchange and RPA correlation energies in the adiabatic-connection fluctuation-dissipation theory, *Phys. Rev. B* **79**, 205114 (2009).
- [80] C. G. Broyden, The Convergence of a Class of Double-rank Minimization Algorithms 1. General Considerations, *IMA Journal of Applied Mathematics* **6**, 76-90 (1970).
- [81] R. Fletcher, A new approach to variable metric algorithms, *The Computer Journal* **13**, 317-322 (1970).
- [82] D. Goldfarb, A family of variable-metric methods derived by variational means, *Math. Comp.* **24**, 23-

- 26 (1970).
- [83] D. F. Shanno, Conditioning of quasi-Newton methods for function minimization, *Math. Comp.* **24**, 647-656 (1970).
- [84] D. R. Hamann, Optimized norm-conserving Vanderbilt pseudopotentials, *Phys. Rev. B* **88**, 085117 (2013).
- [85] J. R. Thomas, B. J. DeLeeuw, G. Vacek, T. D. Crawford, Y. Yamaguchi, and H. F. Schaefer, The balance between theoretical method and basis set quality: A systematic study of equilibrium geometries, dipole moments, harmonic vibrational frequencies, and infrared intensities, *The Journal of Chemical Physics* **99**, 403-416 (1993).
- [86] D. A. Clabo, W. D. Allen, R. B. Remington, Y. Yamaguchi, and H. F. Schaefer, A systematic study of molecular vibrational anharmonicity and vibration—rotation interaction by self-consistent-field higher-derivative methods. Asymmetric top molecules, *Chemical Physics* **123**, 187-239 (1988).
- [87] A. Togo, L. Chaput, T. Tadano, and I. Tanaka, Implementation strategies in phonopy and phono3py, *Journal of Physics: Condensed Matter* **35**, 353001 (2023).
- [88] A. Togo, First-principles Phonon Calculations with Phonopy and Phono3py, *Journal of the Physical Society of Japan* **92**, 012001 (2023).
- [89] L. Levien, C. T. Prewitt, and D. J. Weidner, Structure and elastic properties of quartz at pressure, *American Mineralogist* **65**, 920-930 (1980).
- [90] N. Mounet and N. Marzari, First-principles determination of the structural, vibrational and thermodynamic properties of diamond, graphite, and derivatives, *Phys. Rev. B* **71**, 205214 (2005).
- [91] L. He, F. Liu, G. Hautier, M. J. T. Oliveira, M. A. L. Marques, F. D. Vila, J. J. Rehr, G.-M. Rignanese, and A. Zhou, Accuracy of generalized gradient approximation functionals for density-functional perturbation theory calculations, *Phys. Rev. B* **89**, 064305 (2014).
- [92] X. Gonze and C. Lee, Dynamical matrices, Born effective charges, dielectric permittivity tensors, and interatomic force constants from density-functional perturbation theory, *Phys. Rev. B* **55**, 10355–10368 (1997).